Application of Graphene Within Optoelectronic Devices and Transistors

F.V. Kusmartsev, W.M. Wu, M.P. Pierpoint and K.C. Yung

Abstract Scientists are always yearning for new and exciting ways to unlock graphene's true potential. However, recent reports suggest this two-dimensional material may harbor some unique properties, making it a viable candidate for use in optoelectronic and semiconducting devices. Whereas on one hand, graphene is highly transparent due to its atomic thickness, the material does exhibit a strong interaction with photons. This has clear advantages over existing materials used in photonic devices such as Indium-based compounds. Moreover, the material can be used to 'trap' light and alter the incident wavelength, forming the basis of the plasmonic devices. We also highlight upon graphene's nonlinear optical response to an applied electric field, and the phenomenon of saturable absorption. Within the context of logical devices, graphene has no discernible band-gap. Therefore, generating one will be of utmost importance. Amongst many others, some existing methods to open this band-gap include chemical doping, deformation of the honeycomb structure, or the use of carbon nanotubes (CNTs). We shall also discuss various designs of transistors, including those which incorporate CNTs, and others which exploit the idea of quantum tunneling. A key advantage of the CNT transistor is that ballistic transport occurs throughout the CNT channel, with short channel effects being minimized. We shall also discuss recent developments of the graphene tunneling transistor, with emphasis being placed upon its operational mechanism. Finally, we provide perspective for incorporating graphene within high frequency devices, which do not require a pre-defined band-gap.

Keywords Graphene · Indium-based compounds · Plasmonic devices · Nonlinear optical response · Saturable absorption · Zero band-gap · Pre-defined band gap · Chemical doping · Deformation · Carbon nanotubes (CNTs) · Honeycomb

F.V. Kusmartsev (✉) · W.M. Wu · M.P. Pierpoint
Department of Physics, Loughborough University, Loughborough LE11 3TU, UK
e-mail: f.kusmartsev@lboro.ac.uk

K.C. Yung
Department of Industrial and Systems Engineering, The Hong Kong Polytechnic University, Hung Hom, Kowloon, Hong Kong, China

P. Misra (ed.), *Applied Spectroscopy and the Science of Nanomaterials*,
Progress in Optical Science and Photonics 2, DOI 10.1007/978-981-287-242-5_9

structure · Quantum tunneling · Nanomaterials · Nanotransistors · Optoelectronics · High frequency devices

1 Introductom

Two-dimensional materials have always been considered unstable due to their thermal fluctuations [1, 2], in what were famously referred to as the Landau-Peierls arguments. However, many scientists have not given up hope that such two-dimensional structures exist. In 2004, a research team based in Manchester successfully segregated graphene flakes from a graphite sample via 'mechanical exfoliation' (more commonly referred to as the scotch-tape method) [1, 3–6]. They witnessed a full preservation of graphene's hexagonal honeycomb structure, with astounding electrical, thermal and optical characteristics.

Graphene is an allotrope of carbon—other examples include diamond, fullerene and charcoal, all with their own unique properties. Usually graphene will be found in the form of highly ordered pyrolytic graphite (HOPG), whereby individual graphene layers stack on top of one another to form a crystalline lattice. Its stability is due to a tightly packed, periodic array of carbon atoms [7] (cf. Fig. 1), and an sp^2 orbital hybridization—a combination of orbitals p_x and p_y that constitute the σ-bond. The final p_z electron makes up the π-bond, and is key to the half-filled band which permits free-moving electrons [8]. In total, graphene has three σ-bonds and one π-bond. The right-hand portion of Fig. 1, emphasizes how small displacements of the sub-lattices A and B can be shifted in the z-direction [9].

Moreover, graphene's mode of preparation will have a strong influence upon its overall quality and characteristics. As conducted by Geim et al. [10], mechanical exfoliation consists of gradually stripping more and more layers from a graphite sheet, until what remains are a few layers of graphene. In terms of overall mobility and the absence of structural defects, this method will produce the highest quality material. Other methods such as vacuum epitaxial growth or chemical vapour deposition (CVD), each have their own merits, but will generally lead to inferior quality. For a more in-depth discussion of the available manufacturing methods, one can refer to [1, 11–21].

On the other hand, graphene is highly impermeable [7]—the mobility can become severely compromised upon molecular attachment. Yet, this apparent flaw has immediate applications for molecular sensors. By monitoring the deviation of electrical resistivity [22, 23], one could, for example, envision novel smoke detection systems. So too is graphene more than 100 times stronger than steel [7], possessing a Young's modulus as large as 1 TPa [24]. Together with its outstanding electrical [8], thermal [25–27] and in particular, optical properties [11, 24, 28, 29], graphene has thus become a widely sought after material for use in future semiconducting and optoelectronic devices [12, 30].

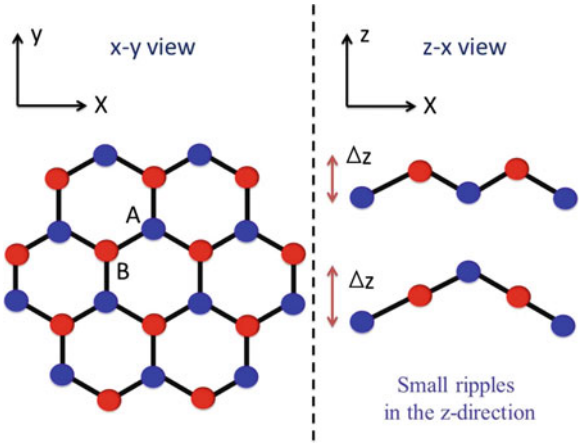

Fig. 1 The honeycomb structure of graphene is presented in the *left-hand* figure. The *right-hand* figure depicts small quantum corrugations of the sub-lattices A and B, which are shifted in the transverse direction by a small fraction of the inter-atomic spacing 'a'

Electrical Mobility—As a material, graphene harbors some remarkable qualities; highly elastic due to its monolayer structure, and more conductive than copper with mobilities reaching up to 2,00,000 $cm^2\ V^{-1}\ s^{-1}$ for perfect structures [24, 31, 32]. Charge carriers in graphene travel with a Fermi velocity $v_F = \sqrt{3}\gamma_0 a/2 \approx 10^6\ ms^{-1}$. Here, $\gamma_0 \approx 3$ eV is the energy required to 'hop' from one carbon atom to the nearest neighbor, $a \approx 1.42$ Å is the inter-atomic spacing between two neighboring carbon atoms, and ħ is Planck's constant [8, 24, 33]. This Fermi velocity is approximately 1/300 the speed of light, thus presenting a miniaturized platform upon which to test many features of quantum electrodynamics (QED) [1]. Theoretical studies with graphene show that the density of states (DoS) of electrons approaches zero at the Dirac point. However, a minimum conductivity $\sigma_0 \sim 4e^2/h$ has been displayed [1], which is approximately double that for the conductance quantum [34, 35]. Even at room temperature, electrons can undergo long range transport with minimal scattering [1, 32, 36].

Thermal Conductivity—Heat flow in suspended graphene was recently shown to be mediated by ballistic phonons, and has been verified by Pumarol et al. [25] with the use of high resolution vacuum scanning thermal microscopy. However, when considering multiple layers of graphene, this transport will be reduced due to an increase of inelastic scattering. The same is observed for graphene coated upon a substrate—the mean free path of thermal phonons degrading to less than 100 nm. Nevertheless, graphene on a silicon substrate can still retain a thermal conductivity of around 600 $Wm^{-1}\ K^{-1}$ [26]—even higher than copper. Whilst the mechanism of heat transport across the graphene-substrate interface remains unknown [37], it is possible this may be linked to the in-plane thermal conductivity [25, 27].

Optical Response—Graphene's atomic thickness makes it almost perfectly transparent to visible light [9, 38], allowing such a material to become widely

accessible to a number of applications. These cover everything from photovoltaic cells, to graphene photonic transistors [30, 33, 39, 40]. Being a single layer of carbon atoms, graphene also exhibits many interesting photonic properties. As such, our focus will be directed mainly upon those which are associated with applications to optoelectronic devices. The transmittance between multiple graphene layers, how optical frequency relates to conductivity, nonlinear optical response, saturable absorption and plasmonics will all be discussed in later sections.

Most semiconducting photonic devices will be governed in some way by electron excitation and electron-hole recombination. Excitation refers to an electron absorbing photon energy of a very specific wavelength within the allowed energy bands. On the other hand, recombination is a process which leads to the emission of photons (cf. electro-luminescence) [38]. Gallium arsenide (GaAs), indium functional compounds and silicon are all common semiconductors for use in photonic devices [41, 42]. However, graphene exhibits a strong interaction with photons with the potential for direct band-gap creation, thus being a good candidate for optoelectronic and nanophotonic devices [43]. Its strong interaction with light arises due to the Van Hove singularity [44]. Graphene also possesses different time scales in response to photon interaction, ranging from femtoseconds (ultra-fast) to picoseconds [43, 45]. Overall, graphene could easily be an ideal candidate for transparent films, touch screens and light emitting cells. It may even be used as a plasmonic device which confines light, and altering the incident wavelength. We shall elaborate upon this in later sections.

2 Energy Spectrum, Band-Gap and Quantum Effects

Theoretical studies of monolayer graphite (i.e., graphene) first began in 1947 by Wallace [8], who considered a simple tight-binding model with a single hopping integral. This model takes into account the hopping of an electron from one carbon atom to its first and second nearest neighbors only. Wallace's conclusions were stark; an electrical conductivity should *theoretically* exist for two-dimensional graphene. To elaborate; at six positions of the Brillouin zone, Dirac points (K and K′) exist. These are points in momentum space for which the energy $E(\mathbf{p}_0) = 0$, where $\mathbf{p}_0 = \hbar\,\mathbf{K}$ (or $\hbar\,\mathbf{K}'$). Here, we have denoted the momentum as a vector $\mathbf{p} = (p_x, p_y) = \hbar\,\mathbf{k}$, where $\mathbf{k} = (k_x, k_y)$ is the wave vector [1]. The energy eigenvalues were found to take a gapless form [8],

$$E^{\pm}(k_x, k_y) = \pm\gamma_0\sqrt{1 + 4\cos\left(\frac{\sqrt{3}}{2}k_x a\right)\cos\left(\frac{1}{2}k_y a\right) + 4\cos^2\left(\frac{\sqrt{3}}{2}k_x a\right)} \qquad (1)$$

where the plus and minus signs refer to the upper and lower half-filled bands respectively [24, 34]. By expanding the above equation in the vicinity of the K or K′ points, one can thus obtain a linear dispersion relation that is given by $E^{\pm} = \pm v_F\,\hbar$

$|\delta\mathbf{k}|$, where $\mathbf{k} = \mathbf{K} + \delta\mathbf{k}$. These constitute what are known as Dirac cones, and are clearly emphasized by Fig. 2. Here, a direct contact of the conduction and valence bands is found [5, 8, 10, 11], thus pertaining to a zero energy band-gap E_g [1, 8, 12]. Therefore, generating a band-gap in graphene will be essential for its application within semiconducting devices (e.g., transistors). On the other hand, graphene may secure its place in high-frequency devices, which do not require a logical OFF state [38].

A. Dirac Energy-Momentum Dispersion

Supposing we consider the Hamiltonian $\hat{H}$ as given by Wallace [8]—in the low energy limit, spinless carriers in graphene possess a zero effective mass, and are well approximated by the relativistic Dirac Hamiltonian $\hat{H}$ [34],

$$\hat{H} = v_F \mathrm{h}\hat{\sigma} \cdot \delta\mathbf{k} \tag{2}$$

where $\hat{\sigma} \cdot \delta\mathbf{k} = \sigma_x \delta k_x + \sigma_y \delta k_y$. Here, $\hat{\sigma} = (\sigma_x, \sigma_y)$ is the vector of 2 × 2 Pauli matrices:

$$\sigma_x = \begin{pmatrix} 0 & 1 \\ 1 & 0 \end{pmatrix} \qquad \sigma_y = \begin{pmatrix} 0 & -i \\ i & 0 \end{pmatrix} \tag{3}$$

The spinor wave function ψ of graphene can be obtained from,

$$\hat{H}\psi = E\psi, \tag{4}$$

where E denotes the energy eigenvalues of $\hat{H}$ [24]. Here, $\psi = (\psi_A, \psi_B)^T$ is a vector containing the two component wave function. These components represent the sublattices A and B accordingly [34].

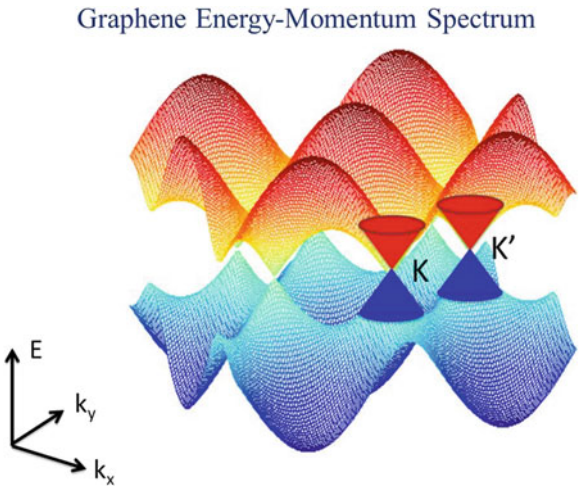

Fig. 2 The energy-dispersion spectrum as given by Eq (1). Here, the z-axis represents the energy $E(\mathbf{k})$, with the x–y plane corresponding to the momentum $\mathbf{k} = (\mathbf{k}_x, \mathbf{k}_y)$. Dirac cones are located at both the **K** and **K′** points of the Brillouin zone

B. Band-Gap Creation

Generally speaking, the electrical conductivity of a material can fall into one of three groups: conductors, insulators, semiconductors [46–48]. For a conductor, electrons are able to move freely in the conduction band since electron states are not fully occupied. However, the conduction and valence band may sometimes be separated by an energy band-gap E_g (e.g., for insulators and semiconductors), thus preventing the free movement of electrons in the conduction band. For an insulator, an electron requires a huge energy in order to excite from the valence to conduction band. A small band-gap is present for semiconductors, with an electronic band structure that is parabolic in shape [12, 31]. Doped semiconductors will make the band-gap even smaller, and hence more easy to control (cf. Fig. 3).

Graphene's high mobility makes it a particularly enticing material for use in electronic devices. However, we have already mentioned that in the vicinity of the Dirac point, graphene possesses a conical band structure which is *gapless* (i.e., $E_g = 0$) [1, 10]. Thus our main concern with regards to logical devices, is the absence of this well-defined OFF state pertaining to zero current flow. To rectify this, we must open up an energy band-gap such that $E_g \neq 0$. With regards to optoelectronic devices, a tunable band-gap can specify the range of wavelengths which can be absorbed. The energy bands for pure graphene, and graphene with a small band-gap E_g are displayed in Fig. 3. The Fermi energy level E_F is situated at the Dirac point for pure graphene [3]. For graphene that has been modified to

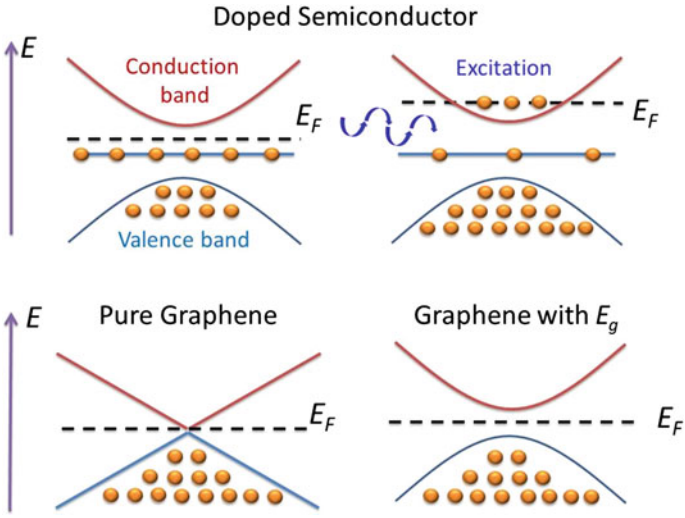

Fig. 3 The *upper half* of this figure depicts the electronic band structure of a doped semiconductor. Typically, the band-gap for a doped semiconductor is very small, with only a small energy being required to excite an electron from the valence to conduction band. The *lower* figure shows the electronic band structure for graphene. For pure samples, no energy band-gap E_g exists. In principle, an energy band-gap E_g can be created via many methods

include a band-gap, an energy is required to excite electrons from the valence to conduction band, and hence an ON/OFF state regime is established [10]. Amongst many others, existing methods include the use of carbon nanotubes (CNTs), graphene nanoribbons (GNRs) or even bilayer graphene [1, 31, 38, 49]. However, it is important to note that although bilayer graphene does possess a zero energy band-gap, an applied electric field can be used to create one [9, 12, 31]. Other methods include deformed structures, graphene oxide (GO) [12, 22, 23], and also the use of chemical doping via compounds such as Boron Nitride (BN) [50, 51]. The idea here, is that the doped atoms alter graphene's honeycomb structure, similar to deformation or localized defects [52, 53]. All in all, one has to note that the aforementioned methods are not well-developed enough to maintain a high mobility. Much more exotic concepts are required, which we shall now discuss.

C. Quantum Phenomena

Of its more surprising attributes, graphene has also displayed signs of anomalous quantum behaviors, even at room temperature [5, 54]. We shall briefly discuss two key phenomena in particular.

Quantum Hall Effect: QHE has been observed for both single and bilayer graphene [11, 55, 56], in the presence of a magnetic field B. The Landau levels for graphene are given by,

$$E_{Landau} = \sqrt{|2e\hbar v_F^2 \mathrm{B}j|} \tag{5}$$

where e is the electric charge, and $j \in \mathbb{Z}$ is the Landau index [5, 54]. In conventional 2-D semiconductors, the Landau levels are $E = \hbar\omega_c\ (j + 1/2)$, where ω_c is the cyclotron frequency [5, 54]. The anomalous energy spectrum for graphene subject to a B field leads to a one half shift of the minimum conductivity at the zero energy Landau level, whereas traditional QHE semiconductors give an integer one [5, 54]. The Hall conductivity σ_{H} is therefore givenby [24, 34],

$$\sigma_H = g\left(j + \frac{1}{2}\right)\frac{e^2}{h} \tag{6}$$

where g is the degeneracy. For graphene, a fourfold degeneracy exists—two spins, and the valley degeneracy of the K and K′ Dirac points [5]. Additionally, the fractional QHE has been observed for both monolayer and bilayer graphene (cf. for details [5, 55, 56]).

Klein Tunneling: Intuition states that if a particle's kinetic energy *KE* is less than some value *U,* then it will be physically incapable of surpassing a potential barrier of the same energy *U*. However, quantum mechanics states that a particle is able to tunnel the potential barrier *U* with a certain decay probability [5]. Furthemore, *relativistic* quantum mechanics permits a remarkable phenomenon called Klein tunneling. Much like a freight train instead taking a tunnel from one side of a mountain to the other, an electron can perform a similar process [54, 57].

This occurs when an electron experiences a strong repulsive force from the barrier *U,* and hence induces a hole inside the barrier [5, 55, 56]. This leads to a matching of the energy spectrum inside and outside the barrier, with the transmission probability becoming very close to one [54]. A perfect transmission is demonstrated for square potentials only, and is dependent upon the energy *KE*, and the angle of incidence θ relative to the barrier [58]. Confined bound states will arise for energies close to the Dirac point [58]. Further details regarding how this confinement effect may relate to the special waveguide geometry has been discussed in references [59–63].

3 Photonic Properties

Optical communication networks are ubiquitous nowadays, affecting our everyday lives. A fiber-optic cable provides a much wider bandwidth, and less energy loss than some traditional copper wiring [41, 42]. According to the Shannon-Hartley theorem [64], the maximum capacity of a channel is given by

$$\max\{C\} = B\log_2\left(1+\frac{P_s}{P_n}\right),$$

where B is the channel bandwidth, and P_s and P_n are the average signal and noise powers respectively. It is therefore obvious that optical cable provides a much larger channel capacity, where $P_s / P_n \gg 1$.

When optical and electronic devices work together (e.g., a modulator), light signals are converted into an electrical equivalent. Generally speaking, the term 'optoelectronic' refers to an optical (photonic) electronic device, which transmits signals via light waves, or electron- photon interaction [41, 42]. A photonic device can be made of semiconductors, either being integrated into electronic circuits or transistors. Optoelectronics also play an important role as the mediator of optical communication. Devices will typically operate with an optical frequency ranging from ultraviolet to infrared (400–700 nm) [41, 42], although graphene photonic devices can possess an even wider spectrum than this [65].

A. Transmittance Properties

As emphasized by Fig. 4, a single layer of graphene absorbs a mere 2.3 % of incident light, allowing around 97.7 % to pass through. Wavelengths typically range from the infrared to ultraviolet regions [33]. The transmittance T of single-layer graphene (SLG) can be approximated by the following Talyor expansion [33, 39, 40, 66, 67]

$$T = \frac{1}{(1+\alpha\pi/2)^2} \approx (1-\alpha\pi) \approx 97.7\,\% \tag{8}$$

where $\alpha = e^2/c\hbar \approx 1/137$ is the fine structure constant. For multiple layers of graphene, this can be roughly estimated by

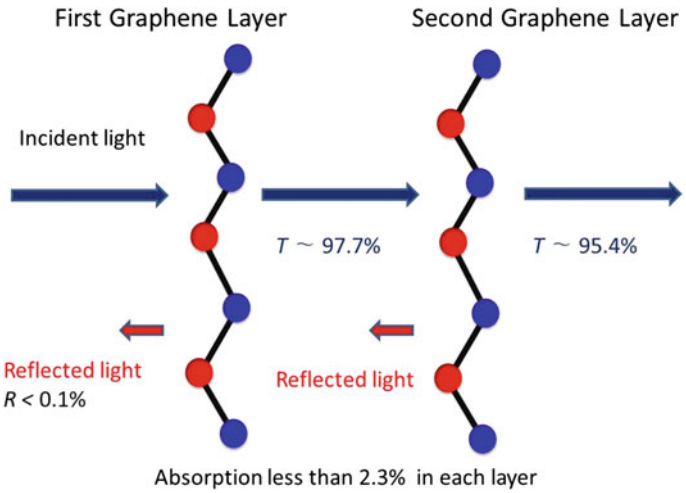

Fig. 4 Incident light passes through the to layers of graphene. The transmission, absorption and reflection coefficients are all shown. Each layer of graphene only absorbs 2.3 % of incident light, transmitting around 97.7 %, and reflecting less than 0.1 %

$$T \approx (1 - N\alpha\pi), \tag{9}$$

where N is number of layers (cf. Bao et al. [39]). For example, the transmittance of bilayer graphene ($N = 2$) is around 95.4 % (cf. Fig. 4). Indium Tin Oxide (ITO) is a semiconductor which is typically used in photonic devices, with a transmittance of around 80 % [33]. It is therefore obvious that graphene film has a clear advantage over ITO. Bonaccorso et al. [33] also point out that the resistance per unit area for ITO is much smaller than for graphene. However, this value can be minimized by increasing the concentration of charge carriers via methods such as doping.

The degree of reflection from SLG is almost negligible, just less than 0.1 % [33]. Avouris et al. [40, 66, 67] also mention that graphene shows a strong interaction of photons, much stronger than some traditional photonic materials per unit depth. It is also surprising that absorption can rise from 2.3 % to around 40 % with high concentration doping [40, 66, 67]. Unquestionably, these properties present graphene as an excellent candidate for use in photonic applications.

B. Optical Conductivity

As mentioned by Avouris et al. [40, 66, 67], graphene possesses a universal optical conductance $G_{op} = e^2/4\hbar$. In general, the optical conductivity σ_{op} depends upon the frequency ω, Fermi energy E_F (via chemical doping or an applied gate voltage), and the transition rate Γ. Moreover, the optical conductivity can be divided into real and imaginary components, $\Re(\sigma_{op})$ and $\Im(\sigma_{op})$ [33, 39, 40, 66, 67],

$$\sigma_{\mathrm{op}}(\omega, E_F, \Gamma) = \Re(\sigma_{\mathrm{op}}) + i\Im(\sigma_{\mathrm{op}}), \tag{10}$$

with energy loss originating from the imaginary part [40, 66, 67].

Bao et al. [39] further explain that the interband and intraband carriers' transitions are the major factors governing the optical conductivity σ_{op} (cf. Fig. 5). Interband transitions refer to an exchange of charge carriers between the conduction and valence bands, whereas intraband transitions refer to a 'jump' between quantized energy levels. For carriers performing an interband transition (at high frequency), the energy of a photon $\hbar\omega$ should be satisfying the relationship $\hbar\omega \geq 2E_F$ [39]. For the low frequency THz range ($\hbar\omega < 2E_F$), the intraband transition would be a significant contribution to the optical conductivity, while interband transitions are prohibited in this range due to the Pauli exclusion principle (Pauli block) [67]. It is important to note that a change in doping concentration would alter the Fermi energy E_F, and hence the optical conductivity. Bao et al. [39] state that one can tune the optical conductivity by controlling the chemical doping (shift of E_F) and the frequency response. However, one must remain aware that a high doping concentration may deteriorate the transmittance T of graphene itself.

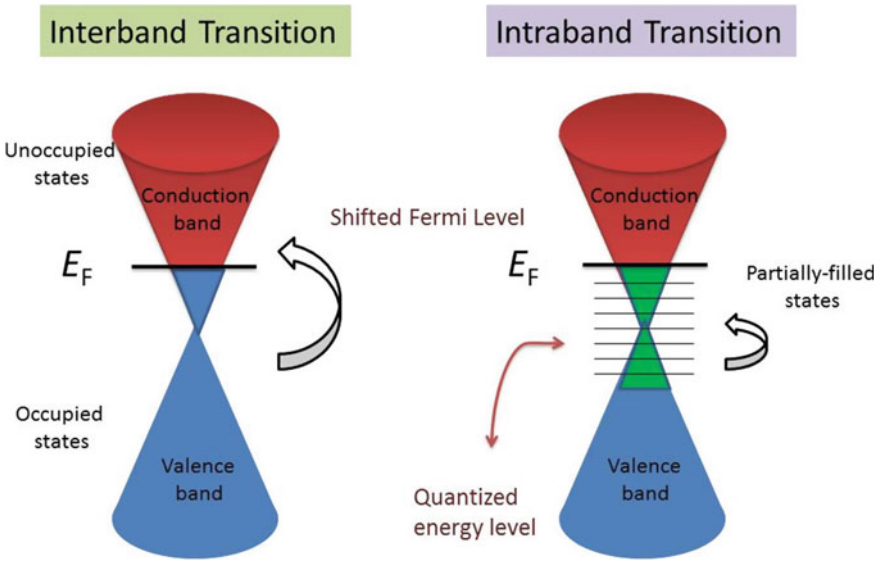

Fig. 5 The Fermi energy level E_F can be shifted upward due to either chemical doping or an applied electric field. Interband transitions refer to an electron 'jumping' from the valence to conduction bands, satisfying the relationship $\hbar\omega \geq 2E_F$. Intraband transitions refer to an electron moving through quantized energy levels, and requires less energy ($\hbar\omega < 2E_F$), provided the states are not already occupied

C. Linear and Nonlinear Optical Response

Graphene also exhibits a strong nonlinear optical response to an electric field, and is an important factor in modifying the shape of the wavefront for incident light [40, 66, 67]. The displacement field D_z is given by the dielectric response of an applied electric field E_z along the 'z' direction, with polarization $P(E_z)$ (cf. Fig. 6);

$$D_z = \epsilon_0 \epsilon_r E_z = \epsilon_0 E_z + P(E_z). \tag{11}$$

Here, ϵ_0 is the electric permittivity of free space, and ϵ_r is the relative permittivity. The polarization response can be written in terms of a power series (cf. for details [39, 68])

$$P(E_z) = C_0 + \epsilon_0 \sum_{j=1}^{\infty} \chi_j (E_Z)^j, \tag{12}$$

where C_0 is a constant associated with the hysteresis (typically $C_0 = 0$), χ_j refers to the dielectric susceptibility of the jth order correction, and $(E_z)^j$ is the j-th power of E_z. The linear dielectric susceptibility χ_1 can again be divided into a real part χ_{R1} and an imaginary part χ_{I1} [39]. The relative dielectric constant can then be expressed in terms of $\epsilon_r = \chi_{R1} + 1$, with an optical refractive index n_{op} given by,

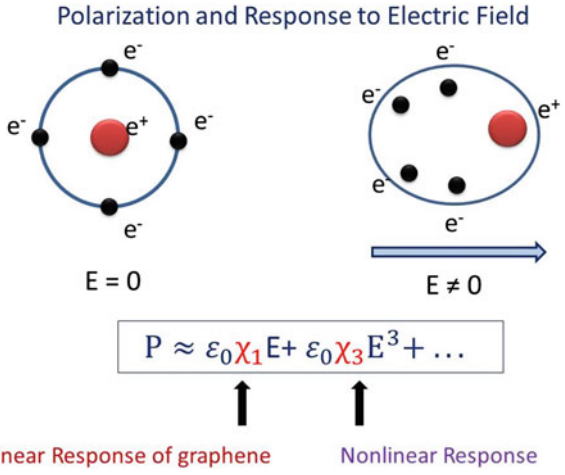

Fig. 6 This figure shows the linear and nonlinear responses to an electric field E. The *left-hand* figure schematically represents an atom without electric field, whilst the *right-hand* figure has a non-zero electric field. The equation is related to the polarization response P. The linear susceptibility χ_1 is usually associated with the refractive index, whereas the nonlinear susceptibility χ_3 provides a unique contribution to the optical properties of graphene. Due to the symmetry of graphene's honeycomb structure, the χ_2 component is very small, and is therefore neglected here

$$n_{op} \approx \sqrt{\epsilon_r} = \sqrt{\chi_{R1} + 1} \tag{13}$$

Thus, the refractive index is determined by the real part of the linear susceptibility χ_{R1}, as mentioned by Bao et al. [39]. Meanwhile, the imaginary part of the linear susceptibility χ_{I1} corresponds to the tangent loss arising at optical frequencies. Bao et al. [39] also come to the conclusion that the 2nd order susceptibility χ_2 is generally small, provided that the symmetry of the graphene honeycomb structure is not broken (i.e., flat). The major contribution to the nonlinear response of graphene originates via the 3rd order term $\epsilon_0 \chi_3 E_z^3$, which modifies the current density in graphene (cf. for details [39]).

D. Surface Plasmons

Surface plasmons describe a set of quantized charge oscillations of electrons and holes, acting upon the graphene-substrate interface [39] (cf. Fig. 7). Plasmons, in general, interact with photons or phonons to form the surface plasmon polariton (SPP). At present, aluminium, silver and gold are all ideal materials for plasmonic platforms [39, 40, 66, 67]. The basic idea is as follows—a dielectric material can be coated upon a graphene layer. Electrons then oscillate on the graphene-substrate interface, excited by the phonon or photon interactions of electromagnetic (EM) fields [39]. The SPP wavelength λ_{SPP} is normally suppressed, and much smaller than the incident wavelength λ_{in}—the ratio of these wavelengths typically being around $\lambda_{in}/\lambda_{SPP} \approx 10$–$100$ [39, 40, 66, 67]. The plasmonic frequency ω_{SPP} on the graphene surface is proportional to the square root of the Fermi energy, as given by [33, 39, 40]

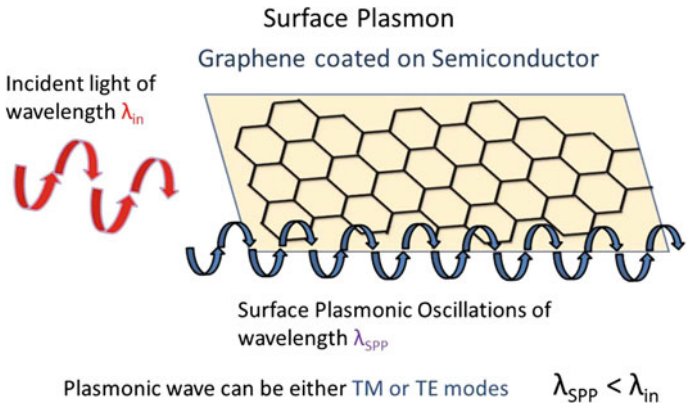

Fig. 7 This figure shows the surface plasmonic wave for graphene coated on a semiconductor. Plasmonic waves are trapped, and oscillate along the graphene and semiconductor interface. Typically, the surface plasmonic wavelength λ_{SPP} will be suppressed, and is much smaller than the incident wave λ_{in}. Either TM or TE wave modes can propagate along the plasmonic surface, depending upon the imaginary component of the optical conductivity

$$\omega_{\mathrm{SPP}} \propto \sqrt{E_F} \propto n^{\frac{1}{4}} \tag{14}$$

where n is a carrier density. In practice, graphene can trap incident light, and an EM wave can propagate along the graphene surface in the THz to infrared range [40, 66, 67]. As mentioned by Avouris et al. [40, 66, 67], the distance traveled for a plasmonic wave in graphene is around $d_{\mathrm{SPP}} \approx 10\text{–}100\ \lambda_{\mathrm{SPP}}$. Graphene is thus a suitable material for a waveguide. Bao et al. [39] further remark that graphene is suitable for guiding transverse magnetic (TM) waves when the imaginary part of the optical conductivity $\Im(\sigma_{\mathrm{op}}) > 0$, and suitable for guiding transverse electric (TE) waves when $\Im(\sigma_{\mathrm{op}}) < 0$.

E. Saturable Absorption and Optical Excitation

There is an interesting property which prevents graphene from absorbing photons at high intensity, and can be used to adjust the wavefront of the light [40, 66, 67]. This is referred to as 'saturable absorption', and is dependent upon the wavelength and incident light intensity. This will be elaborated upon in later sections when we discuss the saturable absorber and photonic (optical) limiter.

The timescale of graphene's response to the interaction of photons, phonons and electron hole recombination can be divided into three regimes [33, 39, 40, 66, 67] (cf. Fig. 8). Graphene has a very quick response to incident photons, around 10–100 fs, whereby 'hot' electrons are excited from the valence to conduction band [33, 39]. This also links to an excitation of the non-equilibrium state. Electrons may then cool down via the intraband phonon emission, with timescales of 0.1–1 ps [40, 66, 67]. Finally, an electron-hole pair may recombine, thus emitting photons, and an equilibrium state being reached. This process takes a mere 1−10 ps. It is important

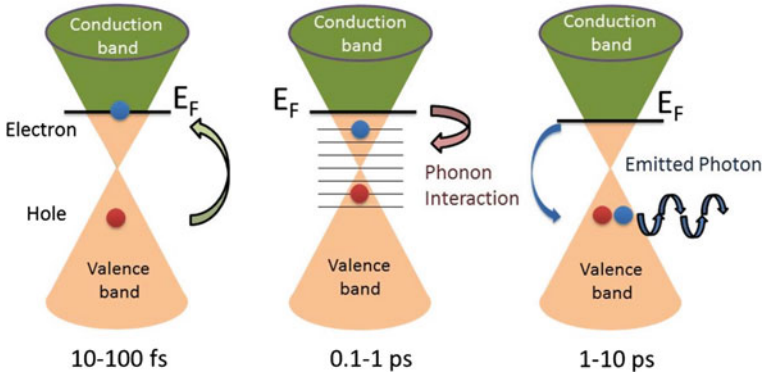

Fig. 8 There are three time scales associated with optical response. The *left-hand* figure represents the inter-band non-equilibrium excitation, and lasts around 10–100 fs. The *middle* figure relates to phonon cooling via the intra-band interaction (0.1–1 ps). Finally, the *right-hand* figure is the process of electron-hole recombination (1–10 ps)

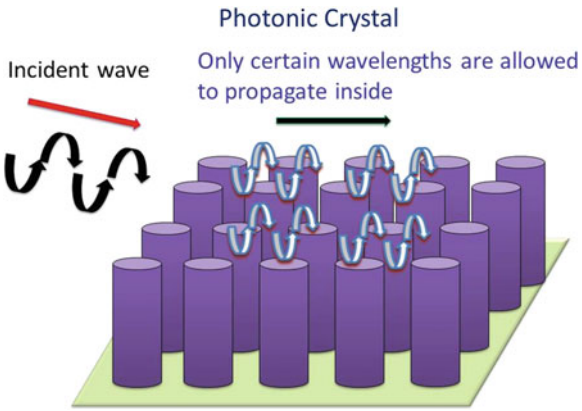

Fig. 9 Here, we present a periodic photonic crystal lattice on the substrate. The lattice forms a band-gap, allowing only certain wavelengths to propagate inside. The photonic properties can therefore be controlled

to note that these excitations and scattering processes are influenced by both topological defects of the lattices (e.g., dislocation and disclination) and boundary characteristics [40, 66, 67].

F. Graphene Photonic Crystal

The photonic crystal is a kind of optical device, whereby a lattice can be periodically allocated upon or within a semiconductor [69, 70] (cf. Fig. 9). A band-gap can be obtained in these periodic structures, and only a certain range of photon energies (i.e., frequencies) are allowed to propagate within. The basic idea is that the periodic dielectric behaves as a superlattice, with restriction being placed upon the wave properties of the electrons [70]. Moktadir et al. [71] find that the graphene photonic crystal provides a wide transmission range, which can be tuned via an applied gate voltage. It has also been reported by Majumdar et al. [72] that the resonance reflectivity can be increased fourfold via a slight 2 nm shifting of the graphene crystalline structure (i.e. dislocations). Graphene's flexible nature therefore offers numerous applications.

4 Graphene Optoelectronic Devices

In this section, we will present ideas for optical devices which incorporate graphene, with emphasis being placed upon their photonic properties. The various photodetectors, optical modulator, and the photonic limiter (mode-locked laser) will all be discussed.

A. Photodiode and Graphene Photodetector

The n-p or p-n junctions are comprised of two different semiconductors (n-type and p-type). Electrons from the n-type semiconductor will flow across the p-type, whereas holes in the p-type will move to the n-type [73]. In any case, a depletion layer is formed at the junction interface. In principle, n-p or p-n junctions can be forward or reverse biased [73]. Since a band-gap can be created in graphene (cf. Sect. 2), it is therefore feasible to conceive of a graphene-semiconductor junction.

Photodiodes are a key component for use in logical devices. It is a current generating device that is sensitive to incoming light (cf. Fig. 10 for the p-n junction configuration). In the absence of light, the device carries a high resistance. However, incoming photons can break down some of the bonding within the compounds at the depletion layer (cf. Fig. 10). Electrons and holes will then be created, and hence a drift current I_d flows across the diode [73]

$$I_d \approx c_1(1 - \exp(-c_2 W_{DL})). \tag{15}$$

Here, c_1 is a constant associated with electric charge and photonic flux, W_{DL} is the width of the depletion layer, and c_2 is a constant associated with the photon energy and band-gap [45].

The working principle of the photodetector is similar to that of the photodiode, transforming photons into an observable current [33, 74] (cf. Fig. 11). More specifically, photons transfer energy to electrons, causing them to 'jump' from the valence band to conduction band (cf. interband transition). This has a typical timescale of ~1 ps [39].

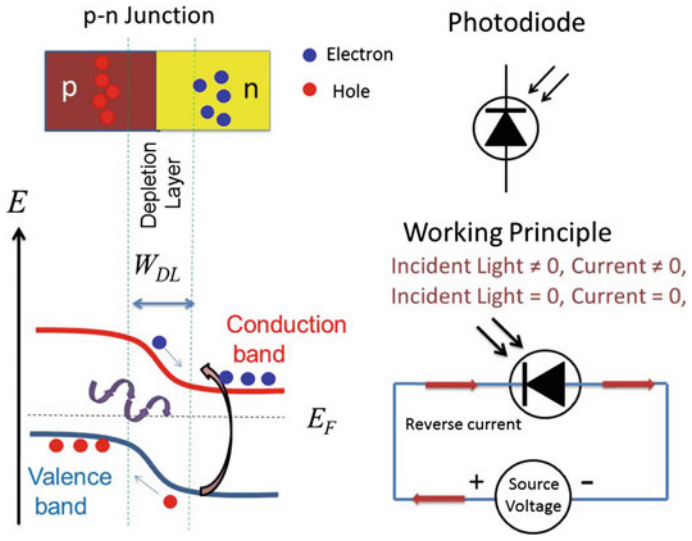

Fig. 10 A schematic of the photodiode is shown. The basic idea is that a reverse current flows upon illumination of the photodiode. The figure also emphasizes that a depletion layer is formed at the interface of the p-n junction

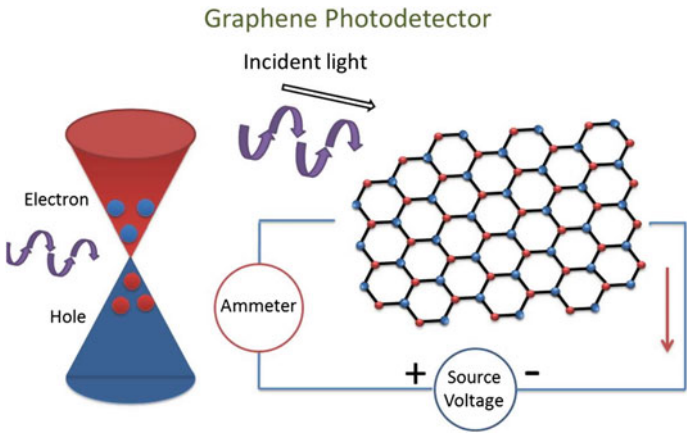

Fig. 11 This figure shows how electrons in the valence band can be excited to conduction band by incident photons. The conductivity of graphene increases, and a measurable current can flow around the circuit. In practice, the idea can be used to measure incident light intensity, for example

$$\gamma(\text{photon}) + e^{-}_{\text{val}} \rightarrow e^{-}_{\text{con}} \tag{16}$$

Here, e^{-}_{val} and e^{-}_{con} refer to electrons in the valence and conduction bands respectively. Bonac-corso et al. [33] point out that the absorption bandwidth of light spectra depends upon the choice of semiconductor. As we mentioned before, graphene interacts with an EM range covering the majority of the visible spectrum [33, 39]. Xia et al. [75] have also reported that the frequency response of graphene can be upwards of 40 GHz, with a theoretical limit reaching even 500 GHz. This response generally depends upon the electrical mobility, resistance and capacitance of the materials [39]. An appropriate bandwidth for graphene can therefore be adjusted via doping or an applied electric field. Mueller et al. [76] further reveal that their results for graphene display a strong photonic response at a wavelength of 1.55 μm, when applying the graphene photodetector on fast data communication links.

Bao et al. [39] have summarized that current from a photodetector can also be generated just by the contact of graphene and a semiconductor, due to the differing work functions and thermal gradient. Current leakage is one of the major drawbacks of the graphene photodetector, although this can be optimized by reducing the band-gap, or coating some dielectric material on the graphene surface [33, 39]. Echtermeyer et al. [77] show that a number of metallic nanoparticles can be allocated on the graphene substrate, vastly improving the efficiency of the devices. The basic idea is that a metallic nanoparticle touches the graphene film, and forms a 'junction like' contact. Metallic nanoparticles on the graphene layer would thus act as small photodetectors at the same time, and thus enhance the sensitivity [77, 78].

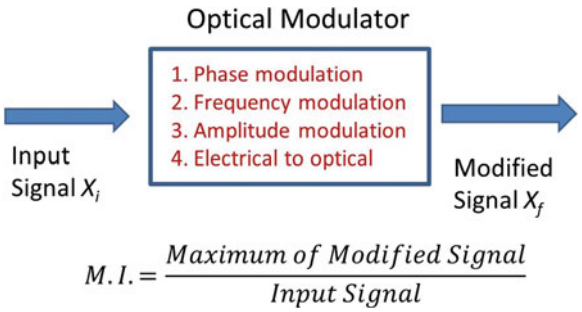

Fig. 12 The optical modulator is an important device for converting electrical signals into an optical equivalent, and therefore an ideal bridge between electronic and optical devices. This device can also change the properties of the incident wave, such as the phase, frequency, and amplitude. The Modulation Index (*M.I*) is defined as the maximum of the modified signal X_f, divided by the input signal X_i

Some other applications such as the measurement of refractive index [79], and the analysis of metamaterials via the graphene sensor [80], are all being studied on the graphene photonic detector platform.

B. Optical Modulator

The optical modulator is a photonic device which transforms electrical signals into an optical equivalent [74, 81, 82] (cf. Fig. 12 for a schematic overview). It is an essential communication link within many electronic devices, and can also alter the properties of light via doping or an applied electric field [39]. For example, assume a plane wave propagates as

$$A = |A|\exp(i\theta), \tag{17}$$

where A can be either electric or magnetic in origin, and θ is the phase of the wave. A modulator changes the amplitude $|A|$ and phase θ of the input wave [39]. Graphene is a suitable material for a modulator since it has a strong response to a wide range of light spectra (i.e., bandwidth) [67, 81, 82]. Typically, graphene will be coated upon the silicon substrate to enhance the absorption rate [67].

Optical modulators can generally be divided into two types [39]. The first is an absorptive modulator, converting photons into some other form of energy. Normally, an absorption modulator can tune the transmitted light intensity via adjustment of the Fermi energy level E_F [39, 67]. The second type is a refractive modulator which can change the dielectric constant according to variation of the electric field. Graphene is a promising material for an absorption modulator due to its wide bandwidth and tunable Fermi energy level [33, 39]. Bao et al. [39] further reveal that the interband transition can be tuned to a logical ON/OFF state, dependent upon E_F. Regardless, graphene provides a high optical Modulation Index (*M.I*), making it an ideal material for any modulator [39]. This index is given by

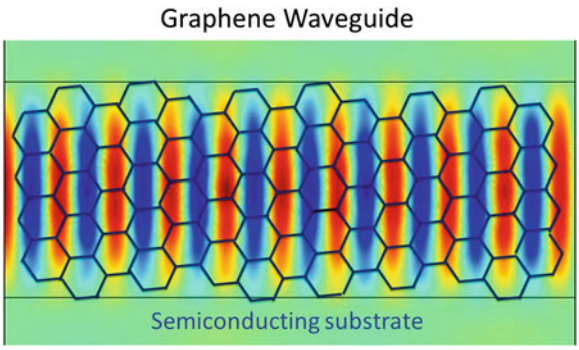

Fig. 13 Graphene is coated upon the semiconducting substrate, and either the TE or TM wave-modes can be transmitted along the graphene thin film

$$M.I. = \frac{\max(X_f)}{X_i}, \tag{18}$$

where X_i and X_f refer to the variable before and after modulation respectively. The graphene modulator can also be applied to the optical resonator, allowing the wavelength to be altered (cf. for details [39]).

Recently, the dielectric sandwich—two layers of graphene with dielectric filling—has been used as an optical signaling modulator [81, 82]. Gosciniak et al. [81] estimate that this graphene optical modulator can reach speeds of up to 850 GHz, with 3 dB modulation and small losses. Liu et al. [82] have also reported a wide absorption range of 1.35–1.60 μm in wavelength.

C. Graphene Waveguide

A waveguide is a physical channel which traps light, guiding it through a designated path [61, 83]. For example, fiber-optic cable is a common waveguide for the communication of light signals—its high refractive index n_{op} trapping light inside the fiber [61]. As we have already seen, the refractive index depends upon the linear dielectric susceptibility χ_{R1} [39]. Zhang et al. [83] have studied the wave-modes of the graphene quantum well, identifying energy dispersion relations associated with Klein tunneling and classical wave-modes [83]. Zhang et al. [83] further note an absence of the 3rd order classical, and 1st order tunneling wave-modes.

Graphene plasmonic waveguides (Fig. 13) have become an essential component for integration with logical devices [84, 85]. Kim et al. [84] have studed the plasmonic waveguide for a dielectric substrate coated on graphene, discovering little optical loss and very fast operating speeds. They show that at the peak wavelength $\lambda = 1.31$ μm, the transmission ratio is around 19 dB for the TM mode [84].

D. Saturable Absorber

As we have already highlighted upon, saturable absorption refers to an absorption of photons decreasing as the light intensity increases [66, 86] (cg. Fig. 14). It is usually applied via the mode-locked laser [39, 87]. Many semiconductors exhibit

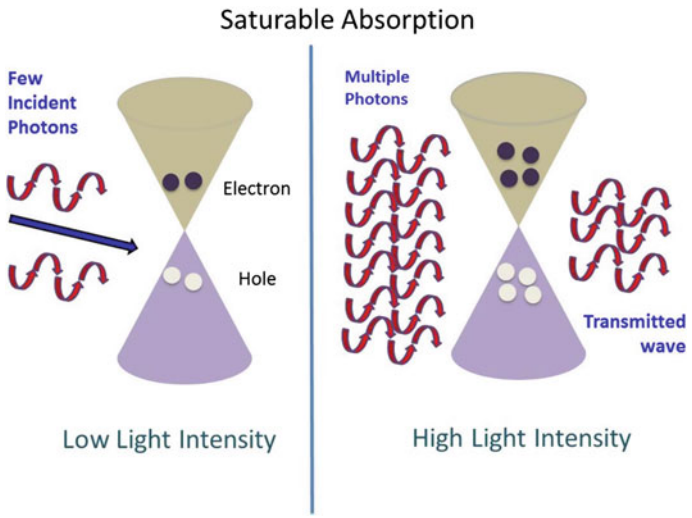

Fig. 14 The idea of saturable absorption for graphene is shown. Graphene can absorb photons, and create electron-hole pairs at low incident light intensity. However, electrons are incapable of occupying the conduction band at high light intensity, since most of the states have already been occupied (cf. Pauli exclusion principle)

saturable absorption, but are not as sensitive as graphene [39, 66]. The basic idea is as follows—a number of excited electrons occupy the conduction band during high intensity exposure, and electrons in the valence band are no longer able to absorb photons due to the Pauli exclusion principle [39, 87]. This property originates from the nonlinear susceptibility of graphene for a short response time [33]. In application, a saturable absorber can be used to transform a continuous wave to a very short wave pulse [33]. Generally speaking, monolayer graphene provides a high saturable absorption coefficient, and recently, some research has uncovered that CNTs may also be suitable candidate for a saturable absorber [86, 88]. Bao et al. [87] also report that a single layer graphene (SLG) saturable absorber can provide around 66 % modulation depth, and produce picosecond wave pulses.

E. Photonic Limiter

A photonic limiter is used to reduce the intensity of light that is emitted from the source [33, 39, 89, 90]. The mechanism is to permit the passage of low intensity light, and to filter out light of higher intensity [89, 90]. Dispersed graphene-oxide solutions are generally used for studying the optical limiter [86, 87]. In particular, graphene, has a strong response to a change of light intensity [39], with a transmittance $T(I)$ that is inversely dependent upon the light intensity I. Such a device can therefore, for example, be implemented to protect the human eye when working with laser apparatus [33]. Wang et al. [89] also note how graphene's nonlinear response is the working principle behind the reduction of light transmitted at high intensity, and also show that graphene can limit a wide range of the visible spectrum [89, 90].

According to Bao et al. [39], the *reverse* saturable absorption (opposite to saturable absorption) is the key nonlinear response that filters high intensity light, and subject to certain conditions. This relates to an optical limiter absorbing more high-energy photons than low-energy photons [39]. Lim et al. [86] have reported that, in practice, the property will change from saturable absorption to reverse saturable absorption, only when microplasmas or microbubbles appear. These lead to a nonlinear thermal scattering, which is also an important factor in limiting high intensity light [39]. Nevertheless, the graphene photonic limiter is still in the early stages of development, with more drastic efforts being required in the near future.

5 Transistors

Nowadays, field effect transistors (FETs) are a key component of most integrated circuitry, commonly acting as a simple logic gate. These devices can be of either n-p-n or p-n-p type, depending upon the desired operation. In this day and age, when the speed and size of devices are becoming all important, scientists are having to seek revolutionary new materials to replace the likes of Silicon (Si), Germanium (Ge) and Gallium Arsenide (GaAs). With outstanding electrical mobility, graphene-based materials are becoming evermore prominent as candidates within future transistors (cf. Fig. 15).

A. Carbon Nanotube Transistor

Before we commence any in-depth discussion of this particular design [22, 23, 91], we must first discuss the physical properties of graphene nanoribbons (GNRs) [92] and carbon nanotubes (CNTs) [38, 93–96]. A GNR is considered to be a piece of graphene of exceptionally narrow width [92]. The electrical attributes of GNRs are determined by their boundary conditions (BCs) (cf. Fig. 16). The 'armchair' BC can cause either metallic or semi-metallic behavior to be exhibited, whereas the zig-zag BC yields only metallic characteristics [38, 93, 94]. Therefore, GNRs are another

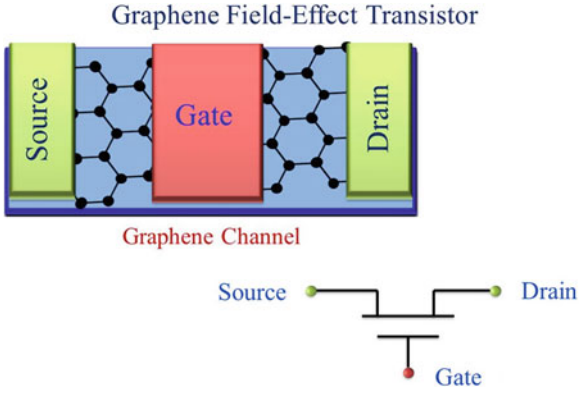

Fig. 15 The idea of the graphene FET is shown. The channel of the transistor is made of graphene, and a gate voltage V_G controls the current flow I_{DS} from drain to source

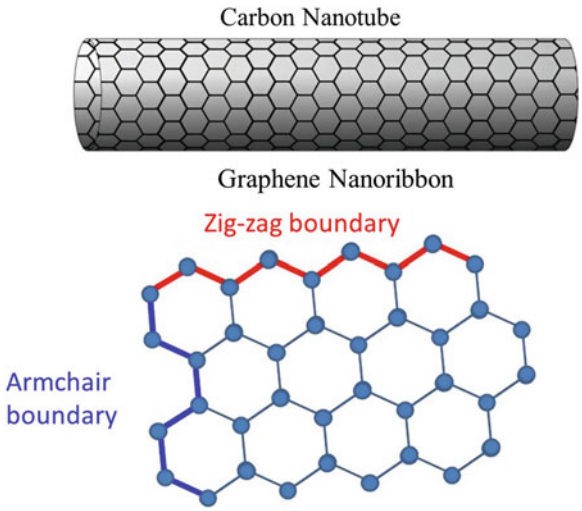

Fig. 16 The lower portion of this figure highlights the two possible boundary conditions (BCs) that a graphene nanoribbon (GNR) can satisfy. The zig-zag BC yields only a conducting state, whereas the armchair BC can either imply a conducting or semiconducting state (dependent upon the width of the nanoribbon). The GNR can also be curled to form a carbon nanotube (CNT), with a band-gap that is inversely proportional to its radius

means of generating an energy band-gap. In this case, the gap size is inversely proportional to the nanoribbon width.

Carbon nanotubes are often considered to be one-dimensional structures, and can be formed by curling a GNR (typically 10–100 nm in width [38, 92]) into a cylindrical configuration (for further details concerning their fabrication, one can refer to [38, 95]). The nanotubes can either be single-walled or multi-walled, although this must be taken into account when considering the CNT radius r_{CNT}. Since this process leads to structural deformation of graphene's honeycomb lattice, there is an overall modification of the electronic band structure [38, 93, 94]. Quantum equivalents of the capacitance, inductance and resistance have all been exhibited within the electrical properties of CNTs, and an energy band-gap E_g is found to be inversely proportional to this CNT radius r_{CNT} [38],

$$E_g \sim 1/r_{CNT}. \tag{19}$$

Thus, together with graphene's capability for long-range ballistic transport (even at room temperature), this presents many useful applications. For example, CNTs would be an apt source-drain channel within semiconducting devices such as transistors [93].

For decades now, the CNT transistor has been subject to intense study [31, 38, 93, 97–99], with a recently reported high switching ratio [99]. They consume much less power, and can possess shorter channel lengths than their silicon-based counterparts. They can also exist in many forms, the most popular being the

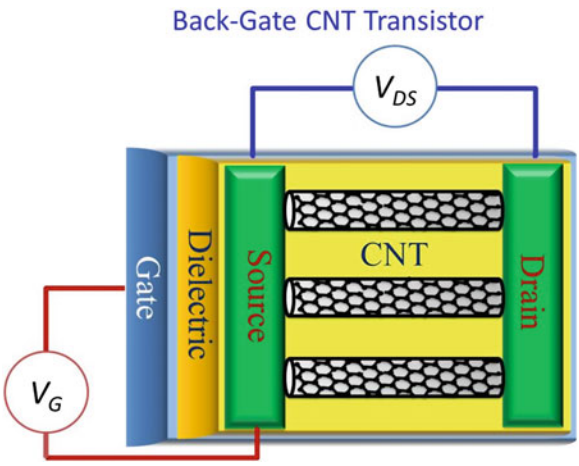

Fig. 17 The figure shows the back-gated CNT transistor. It contains multiple CNTs as the intermediary channels, providing stable performance and current flow. Since the device is back-gated, it can easily be applied within integrated circuitry

top-gate, back-gate and wrap-around gate designs [93, 100–102]. Recently, Shulaker et al. [100] have developed a simple computer from the CNT-based transistors, which can perform more than 20 different instructions. Figure 17 provides a diagrammatic representation of how a back-gated multi-CNT transistor may look—the CNTs themselves acting as the intermediary channels. Currently, one can produce a purified CNT having less than 0.0001 % impurity—which can minimize any inelastic scattering in the channel [101]. The ON/OFF drain-source current I_{DS} can be tuned by using an applied electric field (i.e., the gate voltage V_G) to act upon the CNT channel [101]. Moreover, the ballistic transport of electrons is a result of the one-dimensional CNT structure [38], which again restricts the degree of inelastic scattering. CNT transistors would also appear to alleviate the issue of the short-channel effect in silicon-based devices. In theory, the shorter the channel, the faster the transistor [31, 38]. However, usually when the channel has a length scale in tens of nanometers, the drain-source current I_{DS} tends to become most unstable [38]. A recent study [98, 101] has revealed that the CNT channel can be as short as 9 nm, whilst maintaining a stable current. There are even some predictions that the CNT channel can reach even down to 7 nm in the near future [98, 101].

Schottky barriers at the channel-electrode contacts, are the major obstacle with regards to the CNT's application within transistors [102]. Specifically, they provide a large resistance at the CNT-electrode interface, due to the differing work-functions [38]. The Schottky barrier would generally downgrade the ON/OFF switching ratio [38, 102]. Even worse, this barrier is much larger than for silicon-based devices. A recent study by Javey et al. [102] reveals that the Schottky barrier would be greatly reduced when using the noble metal, Palladium (Pd) as the electrode. They also show that the CNT channel can even then maintain ballistic transport [102]. It is important to emphasize how both classical and quantum equivalents of inductance, resistance and capacitance are exhibited for CNT transistors [38]. In particular, quantum effects become most apparent at the nanoscale. Both quantum

inductance and capacitance are determined by the size, BCs and the density of states (DoS) of the CNT [31, 38], whereas the quantum resistance is equal to $h/4e^2$.

B. Tunneling Transistor

1. *Mechanisms of Tunneling*
   As we have already highlighted upon many times now, the absence of a well-defined OFF state in the graphene transistor is a major setback [103, 104]. Assuming a band-gap were to be created, the next hurdle to overcome is the back-current leakage during this OFF state, since this downgrades the power efficiency [103, 104]. Furthermore, opening this band-gap would then reduce the mobility of graphene, with the Dirac fermions being subject to some inelastic scattering [104].
   The tunneling graphene transistor is a revolutionary new concept, and may be capable of alleviating some of the aforementioned drawbacks. It consumes very little power (up to 10^9 times less than silicon-based devices [105]) and possesses a very fast response time (steep sub-threshold slope) [31]. Michetti et al. also report that an ON/OFF switching ratio can reach as high as 10^4, even with a small electric field [106–108]. It is also found that tunneling occurs at exceptional speed [108]. The underlying concept is visualized in Fig. 18. The interband tunneling is tuned via an applied drain-source voltage V_{DS} and gate voltage V_G [104, 109]. Both V_{DS} and V_G are

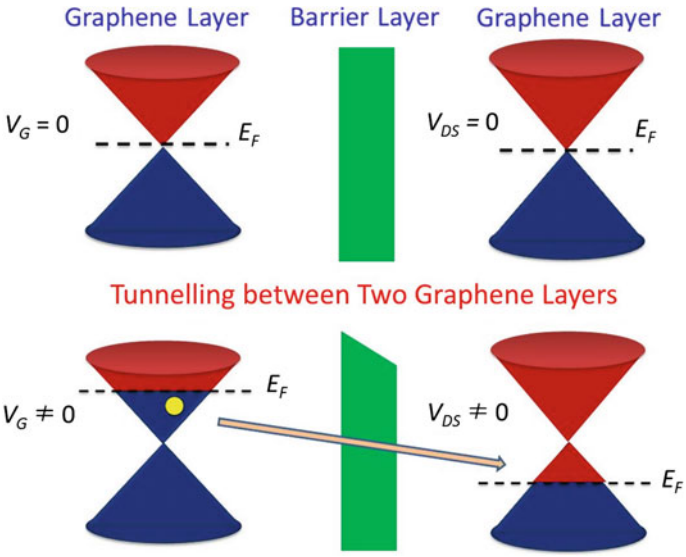

Fig. 18 The *upper* figure shows an intermediate barrier separating the two layers of graphene. In the absence of external electric fields, the Fermi energies are situated at the Dirac points. When the gate voltage V_G and drain-source voltages V_{DS} are applied, electrons begin to accumulate in the conduction band of one graphene layer, and holes in the other. Tunneling can readily occur in this situation, via a fine tuning of both voltages

used to accumulate the electrons and holes in upper and lower graphene layers respectively, and thus altering the shape of the potential barrier [110]. The tunneling is also associated with the channel length, and thickness of the gate oxide layer t_{ox} [106].

2. *Vertical Design*
A relatively new concept which relies upon *vertical* tunneling has been developed by the Manchester research group [103, 104]. The graphene-based device consists of a few (insulating) layers of hexagonal Boron Nitride (hBN) or molybdenum disulphide (MoS_2) [111–113]. These are positioned between two graphene sheets which then constitute the electrodes (cf. Fig. 19). The key point here, is that the insulating layers act as a barrier, and thus preventing the flow of current. As such, there is no need for a well-defined band gap in graphene [111–113]. This has the added benefit of greatly reducing any current leakage whilst in the OFF state [111–113]. The whole process of current tunneling then acts perpendicular to the layers [111–113]. Electrons in the bottom graphene layer will begin to accumulate once a gate voltage V_G is applied across the lower insulating layer [114, 115]. The drain-source voltage V_{DS} is then added to create holes in the upper graphene layer [103, 111–113]. This has the desired effect of increasing the Fermi energy E_F in bottom graphene layer, and decreasing E_F in the upper layer. Electrons in the bottom graphene layer are then capable of tunneling to the top graphene layer [104]. A recent study by Georgiou et al. [111] reveals that the current modulation can reach a high value of 10^6 (even at room temperature). It is also interesting to note that a resonant tunneling within the vertical transistor occurs in some energy states, and a negative differential conductance exists (i.e., current decreases upon an increase in voltage) [112, 113].

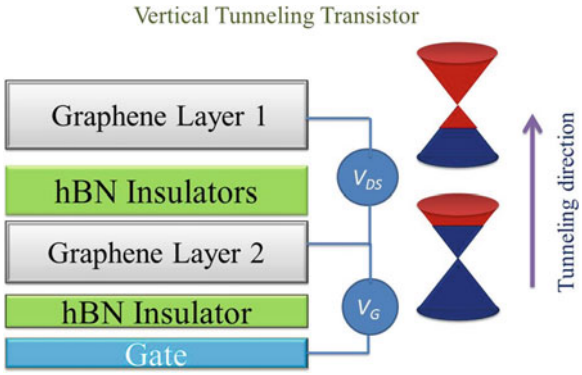

Fig. 19 The vertical tunneling graphene transistor is shown. The hexagonal Boron Nitride (hBN) insulating layers act as an intermediary barrier. The accumulation of holes in the upper graphene layer is controlled by the drain-source voltage V_{DS}, whereas the build-up electrons in the lower graphene layer can be tuned via the gate voltage V_G. Electrons are then capable of tunneling from the bottom to top layer of graphene

C. High Frequency Devices

High frequency transistors do not require an OFF state, and can operate solely through variations of the current or voltage signaling [31, 116]. Graphene may thus be applicable within the realms of high-frequency transistors, inverters, or operational amplifiers [31, 84, 117]. Graphene's response to these signals is incredibly fast, with operating speeds of around a few hundred GHz [84, 116, 118–120].

The performance of high frequency devices is characterized by two important parameters—the cut-off frequency f_{cut} and maximum oscillation frequency f_{max}. The cut-off frequency f_{cut} is given by a current gain G_I equal to unity [116]

$$G_I = 20 \log_{10}\left(\frac{I_{out}}{I_{in}}\right) \tag{20}$$

where I_{out} and I_{in} are the output and input currents respectively. Typically, f_{cut} is proportional to the trans-conductance g_{rf} and the thickness of the gate oxide layer t_{ox}, whereas inversely proportional to the transistor gate length L_G and gate width W_G [31, 116]. The whole expression is given by

$$f_{cut} = c_1 \frac{t_{ox} g_{rf}}{L_G W_G} \tag{21}$$

where c_1 is a constant associated with dielectric gate. In experiments, one would only shorten the gate length L_G for simplicity, thereby increasing the cut-off frequency. Wu et al. [116] report that with CVD-prepared graphene, f_{cut} can reach upwards of 155 GHz for a relatively short gate length of 40 nm. Theoretical simulations have indicated that a cut-off frequency of 1 THz can be attained for just a few nanometers gate length [118].

Similar to f_{cut}, the maximum oscillation frequency f_{max} is obtained for a power gain G_P equal to one. Here, we have $G_P = 10 \log_{10} (P_{out}/P_{in})$, where P_{out} and P_{in} are the output and input powers respectively [116]. The value of f_{max} in graphene-based devices is slightly more complicated, and is dependent upon the cut-off frequency, gate resistances, and the trans-conductance g_{rf} [116, 118]. A recent report [116] has mentioned that f_{max} can reach up to 20 GHz. However, it is important to note that a short gate length would not necessarily imply a high value for f_{max} [116, 118]. At present, not much is understood of the I–V characteristic curve—this has three regions, firstly linear, then saturating, and finally a second linear region [31, 116, 118]. In addition, a change of gate voltage V_G would alter the shape of the I–V curve, and making the saturation region ambiguous. Without a stable saturation region, the value of f_{max} is limited. This problem will require urgent attention in the near future, if the high-frequency transistor is to make any headway [84, 121].

6 Summary

Graphene's outstanding capabilities have drawn the attention of scientists from several interdisciplinary backgrounds—all looking to take advantage. This stand-alone two-dimensional structure is a playground for Dirac fermions which possess a zero effective mass [4, 122, 123]. Quantum phenomena have been observed even at room temperature; a series of anomalous quantum effects including QHE and Klein tunneling [1, 54]. Graphene's versatility is nigh on endless—in this paper, we have merely focused upon optoelectronic devices and transistors. Optical communications provide a much wider bandwidth, with higher efficiencies than most typical conducting wire. We are thus dawning upon a new golden *photonic* age of higher internet speeds, and entertainment-based devices. Graphene's high transmittance, strong interaction of light with ultra-fast response time, wide absorption spectrum, and tunable optical conductivity [33, 39, 67], present an ideal material for optical devices! Amongst many others, these include the photodetector, optical modulator, plasmonic waveguide and also the saturable absorber. The absence of any discernible band-gap for graphene is an unavoidable issue for logical devices, although one may be created via various methods (e.g., structural deformation or chemical doping) [31]. The CNT transistor is now a well-established technology—developed over more than 30 years. Only now has the dream of a CNT-based computer become a working reality [100]. Carriers in CNT channels can perform ballistic transport, even for very short lengths. However, the graphene vertical tunneling transistor is something rather novel. This device itself does not require band-gap at all, and yet, both operates at exceptional speeds, whilst consuming very little power. Our final talking point was the high frequency transistor, which acts as amplifier in the circuit rather than a typical logical device. The cut-off frequency can reach theoretical estimates of up to 1 THz, for just a few nanometers of gate length [38]. Although we have plainly made the case for graphene's implementation within numerous optical and electronic devices, there are a few obstacles which we must overcome. These are the nonlinear *I–V* characteristic curve, and the emergence of Schottky barriers (although we mention a suitable fix). Fifty years ago, no one would have ever envisaged that optical or silicon-based devices would have their place in everyday life. Graphene may change the world!

References

1. Geim AK, Novoselov KS (2007) The rise of graphene. Nature Mater 6:183–191
2. Meyer JC (2007) The structure of suspended graphene sheets. Nature 446:60–63
3. Geim AK (2009) Graphene: status and prospects. Science 324:1530–1534
4. Geim AK (2012) Graphene prehistory. Phys Scr T146:014003
5. Katsnelson MI (2007) Graphene: carbon in two dimensions. Mater Today 10:20–27
6. Novoselov KS et al (2005) Two-dimensional atomic crystals. PNAS 102:10451–10453
7. Savage N (2012) Materials science: super carbon. Nature 483:S30–S31

8. Wallace PR (1947) The band theory of graphite. Phys Rev 71:622–634
9. O'Hare A, Kusmartsev FV, Kugel KI (2012) A stable flat form of two-dimensional crystals: could graphene, silicene, germanene be minigap semiconductors. Nano Lett 12:1045–1052
10. Novoselov KS et al (2004) Electr Field Eff At Thin Carbon Films Sci 306:666–669
11. Novoselov KS (2005) Two-dimensional gas of massless dirac fermions in graphene. Nature 438:197–200
12. Iyechika Y (2010) Application of graphene to high-speed transistors: expectations and challenge. Sci Techno Trends—Q Rev 37:3776–3792
13. Hlawacek G, Beilstein J et al (2012) Imaging ultra thin layers with helium ion microscopy: utilizing the channeling contrast mechanism. Nanotechnology 3:507–512
14. Robinson JA et al (2009) Correlating Raman spectral signatures with carrier mobility in epitaxial graphene: a guide to achieving high mobility on the wafer scale. Nano Lett 9:2873–2876
15. Gouider Trabelsi AB, Ouerghi A, Kusmartseva OE, Kusmartsev FV, Oueslati M (2013) Raman spectroscopy of four epitaxial graphene layers: macro-island grown on 4H-SiC0001 substrate and an associated strain distribution. Thin Solid Films 539:377–383
16. Das A, Pisana S, Chakraborty B, Piscanec S, Saha SK, Waghmare UV, Novoselov KS, Krishnamurthy HR, Geim AK, Ferrari AC, Sood AK (2008) Monitoring dopants by Raman scattering in an electrochemically top-gated graphene transistor. Nature Nanotechnol 3:210–215
17. Bae S et al (2010) Roll-to-roll production of 30-inch graphene films for transparent electrodes. Nature Nanotechnol 5:574–578
18. Chen JH, Jang C, Xiao S, Ishigami M, Fuhrer MS (2008) Intrinsic and extrinsic performance limits of graphene devices on SiO_2. Nature Nanotechnol 3:206–209
19. Bolotin KI et al (2008) Ultrahigh electron mobility in suspended graphene. Solid State Commun 146:351–355
20. Morozov SV et al (2008) Giant intrinsic carrier mobilities in graphene and its bilayer. Phys Rev Lett 100:016602
21. Lin YM, Farmer DB, Jenkins KA et al (2011) Enhanced performance in epitaxial graphene FETs with optimized channel morphology. IEEE Electron Device Lett 32:1343–1345
22. He QY, Wu SX, Yin ZY, Zhang H (2012) Graphene-based electronic sensors. Chem Sci 3:1764–1772
23. He QY et al (2011) Transparent, flexible, all-reduced graphene oxide thin film transistors. ACS Nano 5:082117
24. Neto AHC, Novoselov KS (2011) New directions in science and technology: two-dimensional crystals. Rep Prog Phys 74:082501
25. Pumarol ME et al (2012) Direct nanoscale imaging of ballistic and diffusive thermal transport in graphene nano-structures. Nano Lett 12:2906–2911
26. Prasher R (2010) Graphene spreads the heat. Science 328:185–186
27. Seol JH et al (2010) Science 328:213–216
28. Chen S (2012) Thermal conductivity of isotopically modified graphene. Nature Mater 11:203–207
29. Rafiee J (2012) Wetting transparency of graphene. Nature Mater 11:217–222
30. Engel M et al (2012) Light matter interaction in a micro-cavity controlled graphene transistor room temperature transistor based on a single carbon nanotube. Nature Commun 3:906–911
31. Schwierz F (2010) Graphene transistors. Nature Technol 5:487–496
32. Kusmartsev FV, Tsvelik AM (1985) Semi-metallic properties of a hetero-junction. JETP Lett 42:257–260
33. Bonaccorso F, Sun Z, Hasan T, Ferrari AC (2010) Graphene photonics and optoelectronics. Nat Photonics 4:611–622
34. Sarma SD, Adam S, Hwang EH, Rossi E (2011) Electronic transport in two-dimensional graphene. Rev Mod Phys 83:407–470
35. Zhou YB, Wu HC, Yu DP, Liao ZM (2013) Magneto-resistance in graphene under quantum limit regime. Appl Phys Lett 102:093116

36. Du X, Skachko I, Barker A, Andrei EY (2008) Approaching ballistic transport in suspended graphene. Nature Nanotechnol 3:491–495
37. Koh YK, Bae MH, Cahill DG, Pop E (2010) Heat conduction across monolayer and few-layer graphenes. Nano Lett 10:4363–4368
38. Avouris P, Chen Z, Perebeinos V (2007) Carbon-based electronics. Nature Nanotech. 2:605–615
39. Bao Q, Loh KP (2012) Graphene photonics, plasmonics, and broadband optoelectronic devices. ACS Nano 6:3677–3694
40. Avouris P (2010) Graphene photonics and optoelectronics. Nano Lett 10:4285–4294
41. Saleh BEA, Teich MC (2007) Fundamentals of photonics, 2nd edn. Wiley Series in Pure and Applied Optics. Wiley, USA
42. Kasap SO (2001) Optoelectronics and photonics: principles and practices, 1st edn. Prentice Hall, New Jersey
43. Koppens FHL, Chang DE, Garca de Aba jo FJ (2011) Graphene plasmonics: a platform for strong light-matter interactions. Nano Lett 11:3370–3377
44. Britnell L et al (2013) Strong light-matter interactions in heterostructures of atomically thin films. Sci Comm 340:1311
45. Rosencher E (2002) Optoelectronics, Cambridge University Press
46. Rudden MN, Wilson J (1993) Element of solid state physics. Wiley, New York (Chapter 4–6)
47. Irwin JD, Kerns DV (1995) Introduction to electrical engineering. Prentice Hall, New Jersey Chapter 8–9
48. Turton R (2000) The physics of solids. Oxford University Press, New York Chapter 4–6
49. Kim KS et al (2009) Large-scale pattern growth of graphene films for stretchable transparent electrodes. Nature 457:706–710
50. Fan X, Shen Z, Liu AQ, Kuo JL (2012) Band gap opening of graphene by doping small boron nitride domains. Nanoscale 4:2157–2165
51. Shinde PP, Kumar Y (2011) Direct band gap opening in graphene by BN doping: Ab initio calculations. Phys Rev B 84:125401
52. Coletti C, Riedl C, Lee DS, Krauss B, Patthey L, von Klitzing K, Smet JH, Starke U (2010) Charge neutrality and band-gap tuning of epitaxial graphene on SiC by molecular doping. Phys Rev B 81:235401
53. Terrones H, Lv R, Terrones M, Dresselhaus MS (2012) The role of defects and doping in 2D graphene sheets and 1D nanoribbons. Rep Prog Phys 75:062501
54. Katsnelson MI, Novoselov KS, Geim AK (2006) Chiral tunneling and the klein paradox in graphene. Nature Phys 2:620–625
55. Dean CR et al (2011) Multicomponent fractional quantum Hall effect in graphene. Nature Phys 7:693–696
56. Novoselov KS et al (2007) Room-temperature quantum hall effect in graphene. Science 315:1379
57. Calogeracos A (2006) Paradox in a pencil. Nature Phys 2:579–580
58. Zalipaev VV, Maksimov DN, Linton CM, Kusmartsev FV (2013) Spectrum of localized states in graphene quantum dots and wires. Phys Lett A 377:216–221
59. Hartmann RR, Robinson NJ, Portnoi ME (2010) Smooth electron waveguides in graphene. Phys Rev B 81:245431
60. Williams JR, Low T, Lundstrom MS, Marcus CM (2011) Gate-controlled guiding of electrons in graphene. Nat Nanotech 6:222–225
61. Wu Q, Turpin JP, Werner DH (2012) Integrated photonic systems based on transformation optics enabled gradient index devices. Light Sci Appl 1:e38. doi:10.1038/lsa.2012.38
62. Downing CA, Stone DA, Portnoi ME (2011) Zero-energy states in graphene quantum dots and rings. Phys Rev B 84:155437
63. Stone DA, Downing CA, Portnoi ME (2012) Searching for confined modes in graphene channels: the variable phase method. Phys. Rev. B 86:075464
64. Shannon CE (1949) Communication in the presence of noise. Proc Inst Radio Engs 37:10–21

65. Gan X et al (2013) High-contrast electrooptic modulation of a photonic crystal nanocavity by electrical gating of graphene. Nano Lett 13:691–696
66. Avouris P, Xia FN (2012) Graphene applications in electronics and photonics. Mater Res Soc 37:1225–1234
67. Avouris P, Freitag M (2014) Graphene photonics, plasmonics and optoelectronics. IEEE J Sel Top Quantum Electron. doi:10.1109/JSTQE.2013.2272315
68. Butcher PN, Cotter D (1991) The elements of nonlinear optics. Cambridge University Press, Cambridge
69. Lu L, Cheong LL, Smith HI, Johnson SG, Joannopoulos JD, Soljacic M (2012) Three-dimensional photonic crystals by large-area membrane stacking. Optics Lett 37:47264728
70. Joannopoulos JD, Johnson SG, Winn JN, Meade RD (2008) Photonic crystals: molding the flow of light, 2nd edn. Princeton University Press, Princeton
71. Moktadir Z, Charlton M, Pollard M, Mizuta H, Rutt H (2011) Tunable transmission in a graphene photonic crystal in mid-infrared. In: Graphene 2011 conference, Bilbao, Spain, 11–14 Apr 2011
72. Majumdar A, Kim J, Vuckovic J, Wang F (2014) Graphene for tunable nanophotonic resonators. IEEE Sel Top Quantum Electron 20:4600204
73. Mohan Kumar D (2003) Optoelectronic devices and their applications. Electronics for You, Oct 2003
74. Furchi M et al (2012) Microcavity-integrated graphene photodetector. Nano Lett 12:2773–2777
75. Xia F, Mueller T, Lin YM, Garcia AV, Avouris P (2009) Ultrafast graphene photodetector. Nature Nanotech 4:839–843
76. Mueller T, Xia F, Avouris P (2010) Graphene photodetectors for high-speed optical communications. Nat Photonics 4:297–301
77. Echtermeyer TJ et al (2011) Strong plasmonic enhancement of photovoltage in graphene. Nature Commun 2:458. doi:10.1038/ncomms1464
78. Nicoletti O et al (2013) Three-dimensional imaging of localized surface plasmon resonances of metal nanoparticles. Nature 502:80–84
79. Xing F et al (2012) Sensitive real-time monitoring of refractive indexes using a novel graphene-based optical sensor. Sci Rep 2:908. doi:10.1038/srep00908
80. Amin M, Farhat M, Bagci H (2013) A dynamically reconfigurable Fano metamaterial through graphene tuning for switching and sensing applications. Sci Rep 3:2105. doi:10.1038/srep02105
81. Gosciniak J, Tan DTH (2013) Theoretical investigation of graphene-based photonic modulators. Sci Rep 3:1897. doi:10.1038/srep01897
82. Liu M et al (2011) A graphene-based broadband optical modulator. Nature 474:64–67
83. Zhang FM, He Y, Chen X (2009) Guided modes in graphene waveguides. Appl Phys Lett 94 (21):212105
84. Kim JT, Choi SY (2011) Graphene-based plasmonic waveguides for photonic integrated circuits. Optic Express 19:24557–24562
85. Wang X, Cheng Z, Xu K, Tsang HK, Xu JB (2013) High-responsivity graphene/siliconheterostructure waveguide photodetectors. Nat Photonics 7:888–891
86. Lim GK et al (2011) Giant broadband nonlinear optical absorption reponse in dispersed graphene single sheets. Nat Photonics 5:554–560
87. Bao Q et al (2011) Monolayer graphene as a saturable absorber in a mode-locked laser. Nano Res. 4(3):297–307
88. Hendry E, Hale P, Moger J, Savchenko A, Mikhailov S (2010) Coherent nonlinear optical response of graphene. Phys Rev Lett 105:97401
89. Wang J, Hernandez Y, Lotya M, Coleman JN, Blau WJ (2009) Broadband nonlinear optical response of graphene dispersions. Adv Mater 21:2430–2435
90. Tutt LW, Kost A (1992) Optical limiting performance of C60 and C70 solutions. Nature 356:225–226

91. Park J, Nam S, Lee M, Lieber CM (2011) Synthesis of monolithic graphene-graphite integrated electronics. Nat Mater 98:082117
92. Li X, Wang X, Zhang L, Lee S, Dai H (2008) Chemically derived, ultra-smooth graphene nanoribbon semiconductors. Science 319:1229–1232
93. Tans SJ, Verschueren ARM, Dekker C (1998) Room-temperature transistor based on a single carbon nanotube. Nature 393:49–52
94. Martel R, Schmidt T, Shea HR, Hertel T, Avouris P (1998) Single- and multi-wall carbon nanotube field-effect transistors. Appl Phys Lett 73:2447–2449
95. Zhu HW, Xu CL, Wu DH, Wei BQ, Va jtai R, Ajayan PM (2002) Direct synthesis of long single-walled carbon nanotube strands. Science 296:884–886
96. McCann E, Fal'ko VI (2004) Symmetry of boundary conditions of the Dirac equation for electrons in carbon nanotubes. J Phys Cond Matter 16:2371–2379
97. Kreupl F (2012) Carbon nanotubes finally deliver. Nature 484:321–322
98. Franklin AD et al (2012) Sub-10 nm carbon nanotube transistor. Nano Lett 12:758–762
99. Jang S et al (2010) Flexible, transparent single-walled carbon nanotube transistors with graphene electrodes. Nanotechnology 21:425201
100. Shulaker MM, Hills G, Patil N, Wei H, Chen HY, Wong HSP, Mitra S (2013) Carbon nanotube computer. Nature 501:526
101. Franklin AD (2013) Electronics: the road to carbon nanotube transistors. Nature 498:443
102. Javey A, Guo J, Wang Q, Lundstorm M, Dai H (2003) Ballistic carbon nanotube transistors. Nature 424:654
103. Britnell L et al (2012) Field-effect tunneling transistor based on vertical graphene heterostructures. Science 335:947–950
104. Ponomarenko LA et al (2011) Tunable metal-insulator transition in double-layer graphene heterostructures. Nature Phys. 7:958–961
105. Yang X et al. (2010) Graphene tunnelling FET and its applications in low power circuit design. In: GLSVLSI10 proceedings of the 20th symposium on great lakes symposium on VLSI, pp 263–268
106. Michetti P, Cheli M, Iannaccone G (2010) Model of tunneling transistors based on graphene on SiC. Appl Phys Lett 96:133508
107. Zhao P, Chauhan J, Guo J (2009) Computational study of tunneling transistor based on graphene nanoribbon. Nano Lett 9:684–688
108. Zhang Q, Fang T, Xing H, Seabaugh A, Jena D (2008) Graphene nanoribbon tunnel transistors. IEEE Electron Dev Lett 29:1344–1346
109. Ionescu MA, Reil H (2011) Tunnel field-effect transistors as energy-efficient electronic switches. Nature 479:329–337
110. Nandkishore R, Levitov L (2011) Common-path interference and oscillatory zener tunneling in bilayer graphene p-n junctions. PNAS 108:14021–14025
111. Georgiou T et al (2013) Vertical field effect transistor based on graphene-WS2 Heterostructures for flexible and transparent electronics. Nature Nanotechnol 8:100–103
112. Britnell L et al (2013) Resonant tunnelling and negative differential conductance in graphene transistors. Nature Comm 4:1794
113. Nguyen VH et al (2012) Bandgap nanoengineering of graphene tunnel diodes and tunnel transistors to control the negative differential resistance. J Comput Electron 12:85–93
114. Malec CM, Davidovic D (2011) Transport in graphene tunnel junctions. J Appl Phys 109:064507
115. Cobas E, Friedman AL, Erve OMJ, Robinson JT, Jonker BT (2012) Graphene as a tunnel barrier: graphene-based magnetic tunnel junctions. Nano Lett 12:3000–3004
116. Wu Y et al (2011) High-frequency, scaled graphene transistors on diamond-like carbon. Nature 472:74–78
117. Schall D, Otto M, Neumaier D, Kurz H (2013) Integrated ring oscillators based on high-performance graphene inverters. Sci Rep 3:2592
118. Zheng J et al (2013) Sub-10 nm gate length graphene transistors: operating at terahertz frequencies with current saturation. Sci Rep 3:1314

119. Lin YM et al (2010) 100-GHz transistors from wafer-scale epitaxial graphene. Science 327:662
120. Cheng R et al (2012) High frequency self-aligned graphene transistors with transferred gate stack. PNAS 109:11588–11592
121. Yung KC, Wu WM, Pierpoint MP, Kusmartsev FV (2013) Introduction to graphene electronics—a new era of digital transistors and devices. Cont Phys 54:233–251. doi:10.1080/00107514.2013.833701
122. Pototsky A, Marchesoni F, Kusmartsev FV, Hanggi P, Savel'ev SE (2012) Relativistic Brownian motion on a graphene chip. Eur Phys J B 85:356
123. Yang Y et al (2013) Coherent nonlocal transport in quantum wires with strongly coupled electrodes. Phys Rev B 87:045403